UC Santa Cruz

UC Santa Cruz Electronic Theses and Dissertations

Title

Late Pleistocene Central Equatorial Pacific Temperature Drivers

Permalink

https://escholarship.org/uc/item/3d41w5qn

Author

Yuan, Victoria

Publication Date

2018

Copyright Information

This work is made available under the terms of a Creative Commons Attribution License, availalbe at https://creativecommons.org/licenses/by/4.0/

Peer reviewed|Thesis/dissertation

eScholarship.org Powered by the California Digital Library
University of California

University of California

Santa Cruz

Late Pleistocene Central Equatorial Pacific Temperature Drivers

A thesis submitted in partial satisfaction

of the requirements for the degree of

MASTER OF SCIENCE

in

EARTH SCIENCES

by

Victoria Yuan

June 2018

The Thesis of Victoria Yuan

is approved:

_____

Professor A. Christina Ravelo, Chair

_____

Professor Adina Paytan

_____

Professor James Zachos

_____

Tyrus Miller

Vice Provost and Dean of Graduate Studies

Copyright © by

Victoria Yuan

2018

TABLE OF CONTENTS

LIST OF TABLES AND FIGURES

APPENDIX A. SUPPLEMENTAL TABLES

ABSTRACT

Late Pleistocene Central Equatorial Pacific Temperature Drivers

by

Victoria Yuan

Tropical Pacific sea surface temperatures (SSTs) are a critical component of the global climate system with oceanic and atmospheric teleconnections through meridional and latitudinal heat transport. Understanding the climate drivers and dynamics of this region enables a better understanding of global climate. Orbital scale climate drivers for eastern and western Pacific SSTs have been studied; however, SSTs and thermocline structure have not been studied in the central equatorial Pacific (CEP). Studying temperature dynamics in the CEP upper water column can help determine which mechanisms control SST and thermocline structure and test previously proposed hypotheses. Here, I present CEP SST and subsurface temperature records from the Line Islands (ML1208-17PC) that span the last 380,000 years. Using two species of foraminifera, *G. ruber* and *G. tumida*, I respectively generated Mg/Ca based SST and subsurface temperature records and compared them to published records from the equatorial Pacific. This comparison indicates an expanded west pacific warm pool (WPWP) during interglacial periods but no expansion of the eastern Pacific cold tongue during glacial periods. Based on the thermocline depth proxy, the thermocline was deeper in glacial periods and shallower in interglacial periods. Cross-spectral analysis demonstrates which climate drivers are the likely forcings for CEP SST

and thermocline behavior. The CEP SSTs are distinct from those to the east or the west as they are not directly driven by CO_2 or insolation at orbital frequencies; instead, the CEP SST record is linked to subsurface temperature at eccentricity and obliquity bands. However, changes in thermocline conditions at the CEP are potentially driven by CO_2 and Antarctic temperature changes. This study agrees and supports previous studies that indicate deeper thermocline depths in glacials and shallower depths in interglacials.

DEDICATION

This thesis is dedicated…

In loving memory, to my mother, Wendy Tsai. You are missed dearly.

To my grandmother; you, too, are missed dearly.

To Christina Ravelo, my graduate advisor whom has given me an amazing opportunity to work with and learn from an amazing scientist. Your guidance has been invaluable.

To the friendships made during this journey and extended family that have supported me.

To my committee members, Adina and Jim, who have accommodated the events in my life.

1. INTRODUCTION

Tropical Pacific sea surface temperatures (SSTs) play a critical role in the global climate system by affecting oceanic and atmospheric teleconnections through meridional and latitudinal heat transport (Cane, 1998). Changes in the zonal and meridional gradient of the tropical pacific SSTs have far-reaching effects on precipitation, Walker, and Hadley circulation (Talley et al., 2011). The Late Pleistocene is a dynamic period dominated by 100ky cycles of the growth and decay of large ice sheets. Determining which mechanisms control SSTs during this period when Earth's climate was oscillating between temperature extremes, we can better understand the dynamics of the tropical Pacific.

Previous studies in the east and west equatorial Pacific have looked at a variety of paleotemperature records to determine which climate drivers (e.g. CO_2, insolation) are most likely responsible for changes in tropical pacific SSTs. CO_2 has long been considered the dominant climate forcing for tropical SST in the 100ky world (Herbert et al., 2010), and several studies focusing on the equatorial Pacific have suggested that direct CO_2 radiative forcing is driving the 100ky SST cycles in both the East and West Pacific (Lea, 2004; Lea et al., 2006; Herbert et al., 2010; Dyez and Ravelo, 2014; Dyez et al. 2016). Other climate forcings have been implicated for explaining the variability in equatorial Pacific SST records in the precession and obliquity bands, as CO_2 does not fully account for SST variability at these frequencies (Lea, 2004). To identify the climate drivers contributing to the variability in the west equatorial Pacific (WEP), Dyez and

Ravelo (2014) tested the effect of a number of climate forcings and identified high latitude summer (June 21) insolation as an important climate driver in addition to CO_2. They postulated that high latitude insolation influences the temperature of thermocline source waters; the source waters are subducted at high latitudes and brought to the equatorial Pacific via thermocline circulation. Dyez and Ravelo (2014) identified this to be the most likely mechanism to explain differential cooling between ODP Sites 806 and 871 in the WEP. Dyez et al. (2016) additionally showed that local late autumn (October 1) insolation is also a driver for changes in SST in the cold tongue (ODP Site 846) in the precession band. As explained by Mitchell and Wallace (1992) using modern measurements, SST is influenced by local late autumn insolation through direct radiative forcing as the ITCZ moves north, enabling local insolation to warm the west more than the east. However, ODP Site 1239 and TR163-19, located on the edge of the cold tongue, do not respond to local late autumn insolation. While climate drivers for the cold tongue and WEP have been identified, the understanding of the drivers for temperature change in the tropical Pacific, as a whole, is incomplete. Without a Central Equatorial Pacific (CEP) SST record spanning several glacial-interglacial cycles, we do not know how the CEP responds to mean climate shifts or if the same climate drivers apply.

As mentioned previously, the thermocline plays a crucial role in tropical pacific SSTs; as such, it is necessary to understand mechanistically what changes in the thermocline. Previous studies documenting the thermocline depth during

the Last Glacial Maximum have found that the thermocline shoals in the Eastern Equatorial Pacific (EEP) and the slope of the thermocline is increased, as the thermocline depth in the West Pacific remained deep (Ravelo and Shackleton, 1995; Andreasen and Ravelo, 1997; Patrick and Thunell, 1997; Spero et al., 2003). Philander and Federov (2003) described how the thermocline in low latitude shoals to balance heat loss at high latitude. The application of Philander and Federov's (2003) explanation of how the thermal structure of the ocean responds to changes in latitudinal temperature gradients would predict shallower thermocline depths during glacial periods and deeper thermoclines depths during interglacial periods. Additionally, Philander and Federov (2003) further described how changes in tilt and the latitudinal redistribution of sunlight results in a strong response in the depth of the thermocline. In addition to solar radiation changing the structure of the thermocline, Martinez-Elizade and Lea (2005), based on $\delta^{13}C$ records, suggest increased stratification in the Early Pleistocene (a shoaling of the thermocline) is linked to the cooling of the EEP. Martinez-Garcia et al. (2010) suggest that near synchronous cooling in the sub-Antarctic and sub-Artic and the development of the cold tongue ~1.2Ma provide support for a link between tropical Pacific SST and high latitude SST via circulation and changing conditions at the source area of thermocline water. Despite the number of studies that have invoked this or similar processes to explain the dynamics of the tropical Pacific, records of thermocline conditions spanning multiple glacial-interglacial cycles throughout the region do not exist.

Previous studies in both the EEP and the WEP have proposed mechanisms involving the thermocline and subsurface waters to explain SST records; however, understanding how conditions changed across the expanse of the tropical Pacific has been limited due to the lack of paleoclimate data spanning the Late Pleistocene in the CEP. To test the mechanisms proposed by previous studies involving the thermocline and to better understanding how the CEP is involved in basin-wide dynamics, I have generated magnesium to calcium ratio (Mg/Ca) data from the equatorial site (0°29′N, 156°27′W) of the Line Islands (Figure 1). These newly generated Mg/Ca-based SST, subsurface temperature, and thermocline depth proxy (ΔT) calculated from these records allow us to test previously proposed mechanisms that influence tropical Pacific SSTs.

To infer glacial-interglacial changes in the spatial distribution of SSTs across the equatorial Pacific, the new CEP SST record was compared to existing data from the WEP, at ODP Site 806, and from the EEP at ODP Site 846. An analysis of temperature distributions using a histogram and quantile-quantile plots (Q-Q plots) revealed the convergence of the warmest temperatures for the WEP and CEP but not for the coldest temperatures for the CEP and EEP. This result indicated the expansion of the warmest temperatures during interglacials and the intensification (cooling but probably not expansion) of the cold tongue during glacials. Additionally, the ΔT record from the CEP shows that glacial periods tend to have deeper thermoclines and interglacial periods tend to have shallower thermoclines, supporting previous studies. To determine climate drivers for the

CEP, cross-spectral analysis was used to quantify coherency and phase relations between CEP SSTs, subsurface temperatures, ΔT, and potential climate forcings. The results indicate that the CEP SST record behaves differently from those from the EEP and the WEP. Specifically, CEP SST variability is coherent and in-phase with changes in the thermocline temperature and/or structure, rather than with changes in atmospheric CO_2 forcing. However, in the CEP, thermocline structure is potentially forced by CO_2 or high latitude processes.

2. OCEANOGRAPHIC SETTING

The tropical Pacific is marked by a zonal temperature gradient, with a large warm pool of water in the WEP and a cold tongue prominent in the EEP, which is coupled to a multitude of feedbacks that involve modulation of the strength of the winds, the advection of cool water from the cold tongue to the CEP, the strength of equatorial upwelling, and the formation of clouds. Additionally, these processes are tied to subsurface features, such as the depth of the thermocline. As surface currents flow from east to west, a thick pool of warm water, known as the West Pacific Warm Pool (WPWP), develops in the WEP depressing the thermocline to approximately 200 – 400 m deep. In the EEP, the thermocline is much shallower, allowing upwelling to bring cool waters to the surface and forming the cold tongue. Our study site is located in the CEP at the Line Islands between the WEP and EEP. The Line Islands are approximately between the 155 to 160°W and span from 0.5 to 7°N; this study focuses on the

equatorial site ML1208-17PC (0°29′N, 156°27′W) which is south of the modern seasonal ITCZ shifts. Seasonal temperature changes at the Line Islands are small, <1°C (Schmidtko et al., 2013). Surface water at the equatorial site is slightly cooler and saltier than off the equator due to equatorial upwelling generated by easterly trade winds and moves westward within the South Equatorial Current. Below the surface, there is an eastward flowing Equatorial Undercurrent (EUC) that transports water sourced from the extratropics (Talley et al., 2011).

3. MATERIALS AND METHODS

3.1 Core location and sample resolution

In 2012, R/V Langseth collected a series of cores along the Line Islands Ridge. These cores ran along a North-South transect from 0.5˚N to 7°N. For this project, I selected Site ML1208-17PC (0°29′N, 156°27′W, water depth 2969m) as it has one of the best recoveries, is nearly 8m long, and is located close to the equator thereby recording the effects of upwelling and of changes in the conditions of the EUC and the equatorial thermocline. The core was sampled roughly every 4cm. Samples were freeze dried and then wet sieved to collect the >63μm fraction. Calcite tests of two foraminifera species, surface-dwelling planktic foraminifera *Globigerinoides ruber* and subsurface-dwelling foraminifera *Globorotalia tumida*, were picked. For each sample, 40–100 *G. ruber* (white) tests were picked from the 250–355μm size fraction and 12-40 *G. tumida* tests were picked from the 355-425μm size fraction.

3.2 Age Model

For age control, previously published oxygen isotope data from Lynch-Stieglitz et al. (2015) was fine-tuned to the LR04 stack ten times to constrain age uncertainties for each sample depth and the coretop was set to 4.03ky, based on a radiocarbon date derived from the coretop from an immediately neighboring multi-core (ML1208-14MC). The ten age models generated from the ten tunings results in ten calculated ages for specific sample depths. The variance of each age for each depth is considered the age uncertainty. The average of the ten calculated ages was used to make the final age model.

3.3 Mg/Ca Paleothermometry

Mg/Ca measurements of the two aforementioned species were made. Each sample was prepared and cleaned with oxidative and reductive reagents following established protocols (Boyle and Keigwin, 1985; Mashiotta et al., 1999). Mg/Ca ratios were measured via inductively coupled plasma optical emission spectrometry at the University of California, Santa Cruz (UCSC); 1σ standard deviation for repeated measurements of internal foraminifer reference standards is 0.21 mmol/mol, equivalent to ~0.5 °C.

Measured Mg/Ca values were then converted to temperatures. *G. ruber* Mg/Ca values were converted to SST, using a species specific and tropical Pacific specific equation derived by Dyez and Ravelo (2013); $SST = \ln [(Mg/Ca_{measured} + 0.259 \times Depth\ (km) + 0.537)/0.38]/0.09$. The advantages of this calibration are, in addition to being species specific, it is based on coretop data from the same region

as Site ML1208-17PC, corrects for the effects of water depth dependent dissolution and results in a core-top value of 27.6°C, well within the modern day range. The same calibration is applied to all regional sites with Mg/Ca data discussed in this paper (ODP Site 806 and Site TR163-19) to create internally consistent temperatures. *G. tumida* Mg/Ca values were converted to temperature by applying a dissolution correction (Regenberg et al., 2014) and then using an equation derived by Anand et al. (2003); $T = \ln (Mg/Ca_{corrected} /0.38)/0.09$.

3.4 Spectral Analysis

Cross-spectral analysis was used to quantify coherency and phase via Analyseries software (Paillard and Yiou, 1996) between ML1208-17PC's SST, subsurface temperature, ΔT, high and low latitude insolation, greenhouse gas concentration records, and ice sheet behavior. All records were resampled at even spacing (1 kyr resolution) using piecewise linear integration interpolation in Analyseries, and the Blackman-Tukey method was employed with an 80% confidence interval to find the cross-spectra. This approach establishes dominant frequencies and tests hypotheses about climate forcings for the CEP.

4. RESULTS

4.1 SST, subsurface temperature, and thermocline depth records and distributions

The newly generated Mg/Ca records from the Line Islands equatorial site (Site ML1208-17PC) show cyclicity in both SSTs and subsurface temperatures (Figure 2). The *G. ruber* SST record shows clear glacial-interglacial cycles with

amplitudes of ~3°C between the warmest 10% and coolest 10% of temperatures. The structure of the temperature distribution (Figure 3) of the *G. ruber* SST record shows the majority of Site ML1208-17PC's SSTs are skewed towards the cooler half of the temperature range. The *G. tumida* subsurface temperature record does not show clear glacial-interglacial cycles; however, there is cyclicity in the record that will be discussed in the next section (4.2). Similar to the SST record, the amplitude between the warmest 10% and coolest 10% of temperatures for subsurface temperatures is ~3°C. Unlike SST, the distribution of subsurface temperatures is more evenly distributed, centered on the average.

While the *G. ruber* and the *G. tumida* Mg/Ca records can tell us about past temperatures at the surface and subsurface, the difference between these two temperature records (ΔT=*G. ruber* – *G. tumida*) can serve as a proxy for thermocline depth for the CEP assuming a relatively fixed water depth (100-150m) for *G. tumida* (Ravelo and Shackleton, 1995). A smaller temperature difference would indicate a deeper thermocline because it would imply that the relatively cool thermocline was beneath the depth habitat of *G. tumida*, while a larger temperature difference would indicate that the cool thermocline was sufficiently shallow and closer to the depth habitat of *G. tumida*. ΔT shows clear glacial-interglacial cycles, and, similar to the temperature records, ΔT also has an amplitude of ~3°C between the warmest 10% and coolest 10% of temperatures. ΔT is smaller during cool periods and larger during warm periods, meaning the

thermocline was deeper during glacial periods and shoaled during interglacial periods (Figure 4).

4.2 Spectral and cross-spectral qualities of Site ML1208-17PC records

Examining the spectral quality of the records provides insight into which orbital frequencies dominate the records; furthermore, how these SSTs and subsurface temperatures relate to each other was determined through cross-spectral analysis. The Site ML1208-17PC SST record has variability concentrated at ~100ky (105ky) and 41ky and possibly at precessional periodicities. The spectrum of the Site ML1208-17PC subsurface temperature record has peaks at 100ky (91ky), 42ky, and 20ky (Figure 5). Both temperature spectra show the influence of 100ky glacial-interglacial cycles. The subsurface temperature and SST record at ML1208-17PC were cross-spectrally analyzed to determine if changes in the subsurface temperature may have had a role in determining SST. The results from this analysis showed Site ML1208-17PC subsurface temperatures are strongly coherent and in phase (-3.15 to 1ky) with Site ML1208-17PC SSTs in the band from 35 to 95ky. Additionally, there is weaker, in-phase coherency between the two records at the precession periodicity (23ky). Overall, this suggests that subsurface temperatures and SSTs are correlated at all orbital bands (Figure 6).

As aforementioned in section 4.1, the Site ML1208-17PC ΔT record has cyclicity that is not easily identifiable as glacial-interglacial cyclicity; only after examining the spectral quality, is it clear from the spectrum of the Site ML1208-

17PC ΔT record that thermocline depth behavior (as represented by changes in ΔT) has low-frequency variability, not quite centered at 100ky but still largely influenced/linked to ~100ky climate with a relatively large peak centered at 133ky and spanning eccentricity periodicity of ~100ky (Figure 5). To further examine this proxy for thermocline depth, ΔT and $\delta^{18}O$ from ML1208-17PC were cross-spectrally analyzed to examine how thermocline depth and global climatic changes, as represented by the ML1208-17PC $\delta^{18}O$, are related. These two records have strong, in-phase coherency between 83 to 111ky, supporting the influence of glacial-interglacial (extratropical climate) changes on the tropics (Figure 7) and indicating when $\delta^{18}O$ is high (glacial), ΔT is low (deeper thermocline) and vice versa. Once again, this cross-spectral analysis supports the earlier interpretation that during the glacial periods, Site ML1208-17PC had a deeper thermocline, and, during interglacial periods, Site ML1208-17PC had a shallower thermocline.

5. DISCUSSION

5.1 Glacial Interglacial Patterns in SST spatial patterns and in thermocline structure

To understand the Site ML1208-17PC CEP SST data in the context of the broader equatorial Pacific and to provide insight into changes in spatial patterns on glacial-interglacial timescales, the ML1208-17PC SST record was compared to the SST record from WEP ODP Site 806 (Medina-Elizalde and Lea, 2005) and

the SST record from EEP ODP Site 846 (Liu and Herbert, 2004). The *G. ruber* SST record from ML1208-17PC is the first high resolution record from the CEP to span several glacial-interglacial cycles and the *G. tumida* subsurface record is the first high-resolution record of subsurface temperatures in the equatorial Pacific. To circumvent the possible influence of age model differences on site-to-site comparisons, SST distributions were compared through histograms and Q-Q plots to reveal how the CEP record compares to those of the WPWP and the EEP cold tongue. For example, expansion of the WPWP can be inferred from the amount of warming that occurred at CEP Site ML1208-17PC relative to WEP ODP Site 806, and the changes in the spatial character and intensity of the cold tongue can be inferred by comparing SSTs at Site ML1208-17PC to those at EEP ODP Site 846. Examination of the temperature distributions (Figure 8) indicates that SST maxima at Site ML1208-17PC are similar to those at WEP ODP Site 806 while SST minima at Site ML1208-17PC are notably cooler than SST minima at WEP ODP Site 806. The fact that ODP Site 806 and Site ML1208-17PC have maxima SSTs that converge (Figure 8) indicates that the CEP warmed more than the WEP, enough so that both regions were bathed by similarly warm water suggesting that the WPWP expanded during the very warmest periods (interglacials). Additionally, ODP Site 806 SST values are normally distributed while Site ML1208-17PC SSTs are skewed to the cooler end demonstrating these sites have different dynamical controls on the SST variations. The skewed distribution of SST values at Site ML1208-17PC clearly demonstrates that the

Line Islands were generally cooler compared to the WEP ODP Site 806 except during interglacials when the warm pool expanded eastward into the CEP.

To examine whether changes in the expansion of the cold tongue occurred and was captured by the CEP Site ML1208-17PC SST record, the distribution of SST values from Site ML1208-17PC were compared to the distribution of SST values from EEP ODP Site 846 using a Q-Q plot to determine if the coldest temperatures of these two sites cooled by the same or different amounts (Figure 9). The Q-Q plot indicates that at the cold end of the distribution there was more cooling at EEP Site ODP Site 846 SST than at CEP Site ML1208-17PC. This suggests that during glacial periods the cooling of the EEP cold tongue did not expand westward to the CEP. Alternatively, warming of cold tongue water as it was advected westward to CEP Site ML1208-17PC was more extreme during glacials than other times resulting in warmer waters to the west. To investigate this idea, SST data from Site TR163-19, located in the East Pacific Warm Pool at the northern edge of the cold tongue and north of EEP ODP Site 846, were compared to ODP Site 846 SSTs in a Q-Q plot. This comparison should help to confirm whether the cold tongue intensified (got colder) and/or expanded to the north during glacials. The comparison of the distribution of SSTs from Site TR163-19 with those from ODP Site 846 produced similar results to the comparison of the distribution of SSTs from Site ML1208-17PC with those from ODP Site 846 SSTs; during glacials, EEP cold tongue ODP Site 846 cooled more than at Site TR163-19, which supports the interpretation that the cold tongue

became more intensely cold but did not necessarily expand in its spatial extent (Figure 10).

The regional spatial comparison of SSTs suggests several explanations for the interglacial expansion of the WPWP during interglacial periods and the intensification of the cold tongue during glacial periods: a) wind-driven upwelling could have been more intense during glacial periods, producing colder SSTs at the equator relative to off-equator sites as evidenced by the ODP Sites 871-806 SST difference (Dyez and Ravelo, 2014) and by the TR163-19 and ODP Site 846 difference, b) the thermocline was shallower during glacial periods, allowing colder water to upwell causing a colder and more intensified cold tongue, and/or c) the thermocline was not shallower, but rather colder during glacial periods, allowing colder water to upwell and create a more intensified cold tongue. The first explanation cannot be tested until better proxy records for wind strength in this region and across the studied time interval become available. The second explanation is not supported by ML1208-17PC thermocline depth data or by previous studies. In fact, the ML1208-17PC ΔT record (Figure 4) and cross-spectral results (Figure 7) indicate that the thermocline was deeper during glacial periods and shallower during interglacial periods. Previous studies, such as Ravelo and Shackleton (1995) and Spero et al. (2003), that focused on changes in the tropical Pacific thermocline using isotopic data from the EEP also demonstrate that the thermocline was deeper during glacial periods than interglacials, in agreement with my ML1208-17PC ΔT results. Thus, the third

possible explanation, that the thermocline was cooler, is the most likely underlying explanation for the contraction of the WPWP and intensification of the cold tongue in glacial periods. Furthermore, the *G. tumida* subsurface temperature record contains 100ky periodicity, indicating similarities between thermocline temperatures and SST on glacial-interglacial timescales. In sum, the implications of a shallower thermocline and expanded WPWP during interglacials, and a deeper thermocline and intensified cold tongue during glacials, implies that it is the temperature of the thermocline and/or the strength of upwelling, rather than thermocline depth that may play a role in equatorial Pacific SST dynamics on these time scales.

5.2 Examining Climate Forcings

Previous studies of tropical Pacific SST variability in the EEP and WEP have found atmospheric CO_2 to be the dominant climate forcing during the 100ky world and proposed that it is an expected basin-wide climate forcing (examples: Medina-Elizalde and Lea, 2005; Dyez et al., 2016); this hypothesis can be tested using cross-spectral analysis of Site ML1208-17PC SST and CO_2. Coherent and in-phase relationships suggest a potential direct climate forcing and response; incoherent or out of phase relationships can rule out direct climate forcings. Similar to EEP and WEP records, Site ML1208-17PC SST is strongly coherent (>80%) with CO_2 from 37 to 200ky, 23 to 28ky, and 14.3 to 16.3ky; however, Site ML1208-17PC SST leads CO_2 at all frequencies, specifically by 4.8 to 8.8ky from 37 to 100ky (Figure 11a). This SST lead in the eccentricity band is

unexpected; although, the SST lead over CO_2 has been reported at higher frequencies in previous studies (Lea, 2004; Dyez et al., 2016). Since this is an unexpected finding, the possible effects of tuning the planktonic $\delta^{18}O$ to the LR04 benthic $\delta^{18}O$ stack, as the basis for the age model at Site ML1208-17PC, needs to be considered. Since SST variations lead benthic $\delta^{18}O$ variations in the tropics (Lea et al., 2000), it is possible that planktonic $\delta^{18}O$ changes should lead changes in the global benthic $\delta^{18}O$ stack because the planktonic $\delta^{18}O$ record has a component of change related to SSTs. Tuning the planktonic $\delta^{18}O$ record to the LR04 benthic $\delta^{18}O$ stack could therefore result in erroneous shifts to younger ages and would result in an apparent lag in Site ML1208-17PC records. Thus, this possible shift in age resulting from the use of the planktonic $\delta^{18}O$ data for the age model, cannot explain the observation that Site ML1208-17PC SST variations lead CO_2 variations.

Insolation, at local and high latitudes, has also been found to be a climate forcing that controls EEP and WEP SSTs and can now be tested as a climate forcing for CEP SSTs. High latitude insolation may play a role in equatorial Pacific dynamics through its influence on the temperature of mode water, subducted at high latitude, which is brought to the equatorial Pacific surface through circulation and upwelling of thermocline water. Dyez and Ravelo (2014) showed that there are in-phase relationships between East and West Pacific SSTs and northern hemisphere summer insolation (June 21st, 65°N) in the precession band. At Site ML1208-17PC, equatorial upwelling can bring thermocline waters

to the surface making northern hemisphere summer insolation a likely climate forcing for CEP SSTs on precessional timescales. In Dyez et al. (2016), local October insolation was found to directly influence the cold tongue SSTs. The equatorial Pacific experiences asymmetric heating during boreal autumn due to the shift in the ITCZ. During boreal autumn, the ITCZ shifts north in the EEP and remains near the equator in the WEP. While October insolation might thus be expected to force changes in cold tongue temperature, local October insolation is not expected to be a climate driver at ML1208-17PC as it is south of the ITCZ seasonal shifts (Alder et al., 2003); even EEP sites outside of the modern edge of the cold tongue (Site TR163-19 or ODP Site 1239) were not directly influenced by October insolation. Cross-spectral analysis of Site ML1208-17PC SST with high latitude summer insolation and with local October insolation demonstrates that high latitude summer insolation is only weakly coherent with Site ML1208-17PC SST during obliquity and leads changes in SST by 1.7 to 5.4ky, and local October insolation is not coherent with SST (Figure 11b-c). From these tests, it appears that high latitude summer insolation cannot be conclusively interpreted as directly forcing Site ML1208-17PC SST; however, local October insolation does not influence CEP SST on orbital scales.

In addition to high latitude insolation, high-latitude climate has the potential to alter tropical Pacific SSTs through atmospheric-oceanic teleconnections. Warming and cooling at high latitudes and the growth and decay of ice sheets may change the pole-to-equator temperature gradients and affect

wind strength and upwelling in the tropics. Two additional records were considered to assess this, remote ice sheets (Lisieki and Raymo, 2005) and Antarctic temperature (Jouzel et al., 2007). Site ML1208-17PC SST is strongly coherent with remote ice sheets (LR04) from 23.3 to 400ky and 14.3 to 17.1ky and leads at all coherent frequencies (Figure 11d). Similar results were obtained using Antarctic temperature instead of the LR04 ice volume record (Figure 11e). The leading relationships between Site ML1208-17PC SST and two high latitude climate indicators suggest that equatorial Pacific SST change precedes high latitude climate change, an interpretation supported by previous studies focused on the WEP (Medina-Elizalde and Lea, 2005; Dyez and Ravelo, 2014).

In sum, an examination of previously proposed climate forcings for tropical SST changes demonstrates that none are in phase with Site ML1208-17PC SST; instead, Site ML1208-17PC SST is coherent and in-phase only with the Site ML1208-17PC subsurface temperature record. As previously mentioned, Site ML1208-17PC SST is strongly coherent and in-phase with subsurface temperatures obtained from *G. tumida* from 35 to 95ky and weakly coherent and in-phase in the precession band (Figure 6). This indicates that, in the CEP, SST is directly influenced by upwelling of thermocline water.

It is necessary to understand the cause for changes to thermocline temperature and thermocline depth on orbital cycles since the dynamics that control the thermocline play a significant role in determining SST at orbital scales. As such, Site ML1208-17PC tumidaT (a proxy for subsurface temperature,

which can be related to several processes) and ΔT (a proxy for thermocline depth) were each compared to potential climate forcings using cross-spectral analysis. Similar to Site ML1208-17PC SST, tumidaT and ΔT have the most power in a low frequency peak, ~91ky and ~133ky, respectively. Subsurface temperature (tumidaT) can vary for many reasons such as changes in thermocline temperature and changes in upper ocean mixing. Therefore, we need to examine both local and extratropical drivers as both have the potential to influence this record. ΔT, as a proxy for thermocline depth, can also be influenced by extratropical and local drivers. The results from cross-spectral analysis of ML1208-17PC subsurface temperatures with local and extratropical drivers indicate that high latitude summer insolation is in-phase with subsurface temperatures during obliquity and slightly leads in precession (Figure 12b) while all other potential climate forcings were not in-phase and ruled out (Figure 12a, c-e). This suggests that extratropical solar insolation in mode water formation areas may directly influence mode water and thermocline temperature, a signal that is then advected in the subsurface to the equatorial Pacific. As with ML1208-17PC SSTs, tumidaT is not directly forced by high-latitude summer insolation during precession; nonetheless, obliquity, possibly through its impact on annual average insolation at extratropical latitudes, influences subsurface temperatures. Thermocline depth, ΔT, is in phase with CO_2 from 83.3 to 133.3ky and with Antarctic temperature from 95.2 to 153.8ky (Figure 13a,e) and leads changes in LR04 (Figure 13d). This indicates that the depth of the thermocline responds to both CO_2 radiative forcing and

southern high latitude climate changes. Cross-spectral analyses indicates that ΔT is not coherent with local October insolation or high latitude summer insolation (Figure 13b-c). In sum, while subsurface temperatures are driven by high latitude insolation, thermocline depth may be driven by radiative forcing from CO_2 and southern high latitudes climate changes, potentially in the form of shifted atmospheric circulation, on eccentricity time scales.

6. CONCLUSIONS AND IMPLICATIONS

The implications of these finding are that CEP SST variability is different than SST variability in the EEP and the WEP and is largely influenced by thermocline conditions. Unlike other equatorial Pacific sites, ML1208-17PC SST is not directly driven by CO_2. The thermocline structure at Site ML1208-17PC is, however, potentially influenced by CO_2 and southern high-latitude climate. Neither high latitude summer insolation nor low latitude late autumn insolation are a direct forcing for changes in ML1208-17PC SST or thermocline depth. However, high latitude summer insolation is in-phase with subsurface temperatures during obliquity and leads SST and subsurface temperature during precession, leaving this a potential driver. From these tests, SSTs at Site ML1208-17PC are linked to subsurface temperature and thermocline depth at orbital scales for eccentricity and obliquity, while thermocline structure at Site ML1208-17PC is potentially driven by CO_2 and Antarctic temperatures. This idea of extratropical changes influencing equatorial Pacific SST through changes in the thermocline is supported by previous studies that have examined equatorial Pacific SSTs

changes with changes in the source area of thermocline water formation (Dyez and Ravelo, 2014; Martinez-Garcia et al., 2010). Furthermore, ΔT, thermocline depth proxy, at Site ML1208-17PC supports equatorial Pacific thermocline deepening in glacial periods (Ravelo and Shackleton, 1995; Andreasen and Ravelo, 1997; Patrick and Thunell, 1997; Spero et al., 2003).

ACKNOWLEDGEMENTS

I would like to thank Sarah White for teaching me foraminifera identification, Mg/Ca sample preparation for the OES, how to run the OES, export and process data, and general insight and discussions about all things tropical Pacific, Rob Franks for setting up and maintaining the OES and being a general resource for all things technical, Colin Carney and Dyke Andreasen for isotope analysis. The age model was generated by Gerald Rustic. Funding was provided by NSF grants awarded to Christina Ravelo. I would also like to thank my committee for their insight.

FIGURES

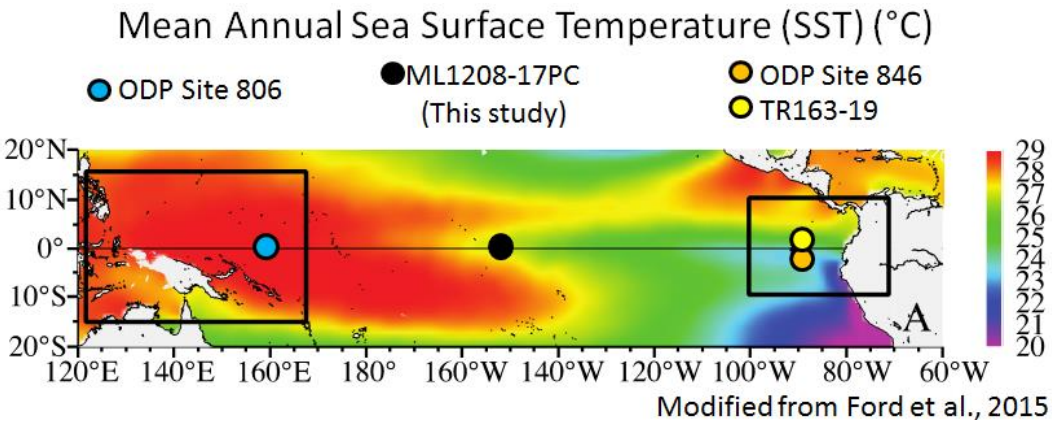

Figure 1 Mean Annual Sea Surface Temperature Map of Equatorial Pacific Modified from Ford et al. (2015). Mean annual sea surface temperature map with the sites discussed plotted.

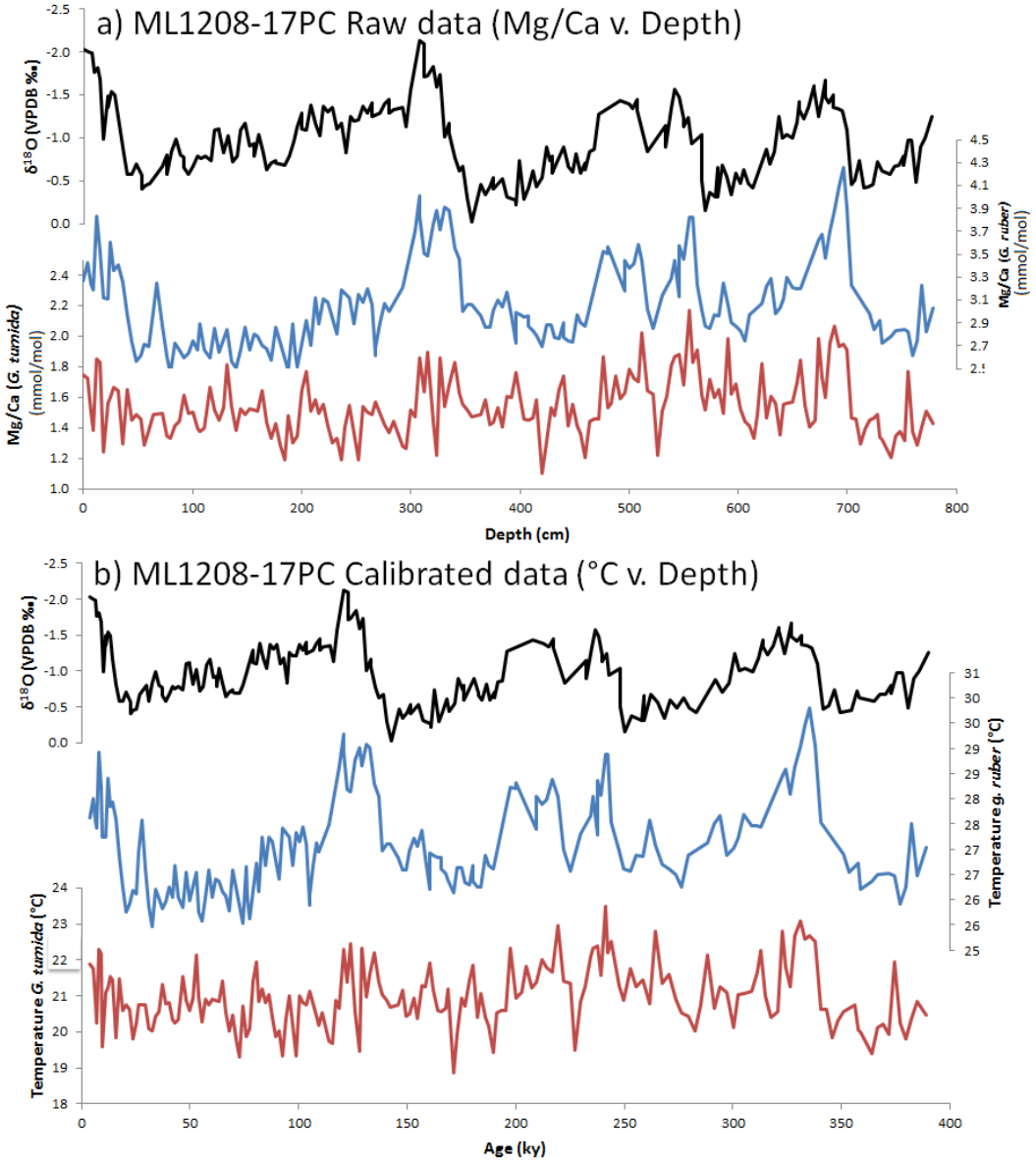

Figure 2 ML1208-17PC Mg/Ca and $\delta^{18}O$ data
a) Mg/Ca from *G. ruber* and *G. tumida* (this study) and $\delta^{18}O$ data from Lynch-Steiglitz, et al. (2015) plotted against depth. b) Calculated temperatures from Mg/Ca from *G. ruber* and *G. tumida* (this study) and $\delta^{18}O$ data from Lynch-Steiglitz, et al. (2015) plotted against depth.

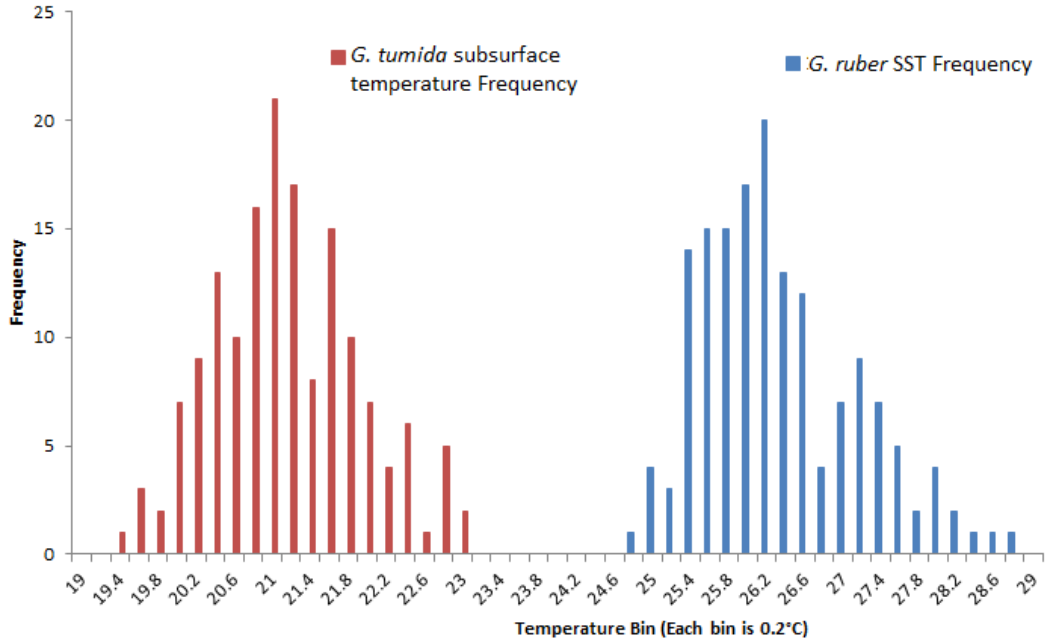

Figure 3 ML1208-17PC Temperature Histograms
Histograms (bins of 0.2°C) of SST and subsurface temperatures from ML1208-17PC. Subsurface temperatures are in red; note the more normal distribution of temperatures. SST temperatures are in blue; note the skew towards cooler temperatures.

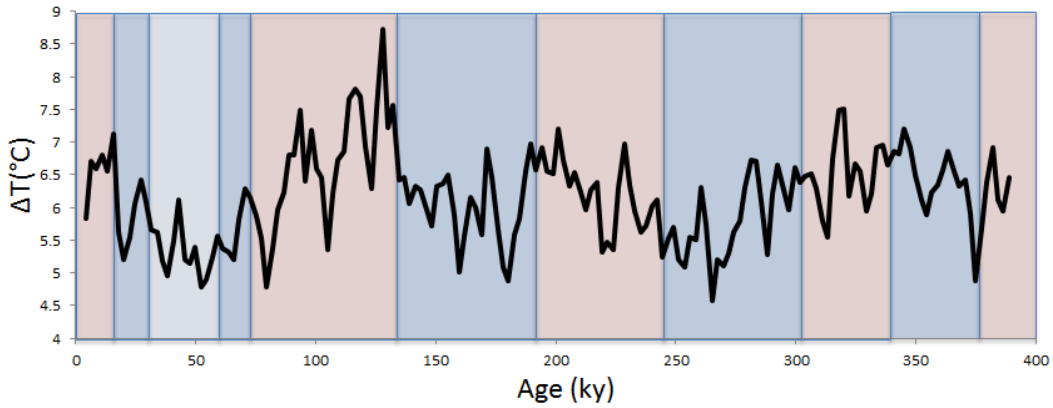

Figure 4 ML1208-17PC Temperature Difference (ΔT)
ΔT, the temperature difference between SST and subsurface temperature, plotted against age. Blue shading indicates glacial periods or cool interglacials. Red shading indicates interglacial periods. Generally, ΔT is smaller in glacial periods and larger in interglacial periods reflecting a deeper thermocline in glacial periods and a shallower thermocline in interglacials periods.

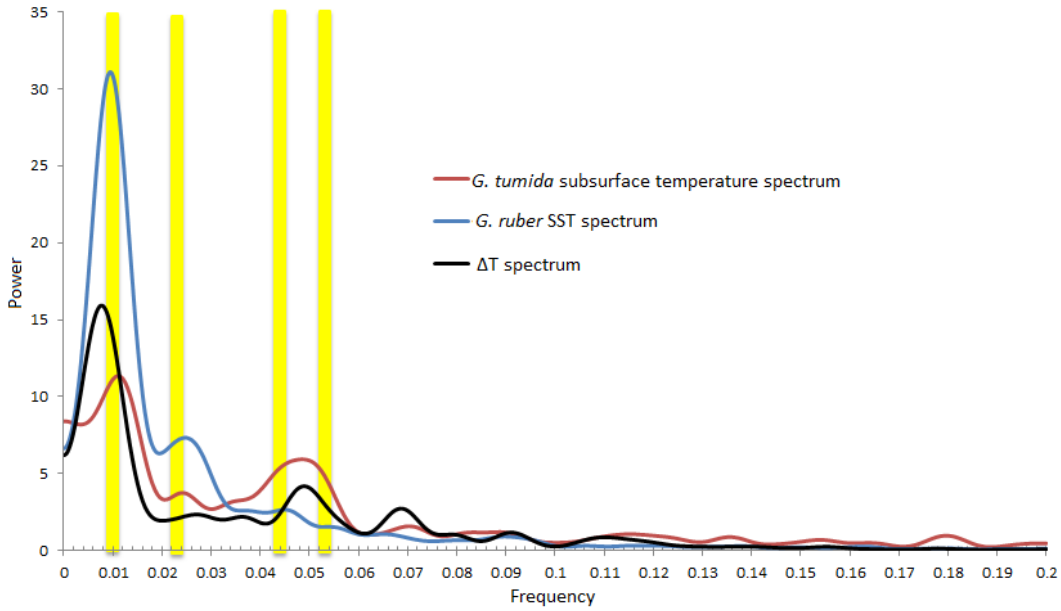

Figure 5 Spectra of ML1208-17PC records

The spectra for Site ML1208-17PC's SST, subsurface temperature, and ΔT records are plotted together. Yellow bars indicate frequency band for orbital cycles at 100ky, 41ky, 23ky, and 19ky. SST has peaks in 105ky, 41ky, and a slight shoulder in precession. Subsurface temperature has a 91ky peak, a 42ky peak, and 20ky peak. ΔT has peaks in 133ky, 20ky, and 15ky.

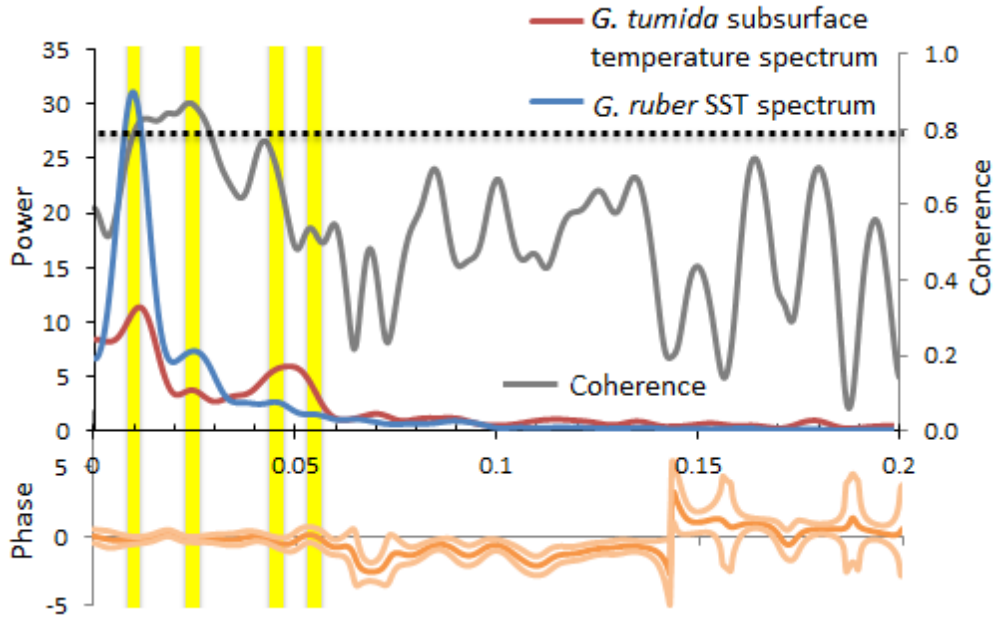

Figure 6 Cross-spectral analysis of SST and Subsurface Temperatures
Cross-spectral analysis of ML1208-17PC SST (blue) and subsurface temperature (red). Coherence is plotted in dark gray; dashed line represents limit of nonzero coherence at 80% confidence interval. Phase is plotted in orange with upper and lower bounds plotted in light orange. Yellow bars indicate frequency band for orbital cycles at 100ky, 41ky, 23ky, and 19ky. The two records are coherent and in-phase from 35 to 95ky.

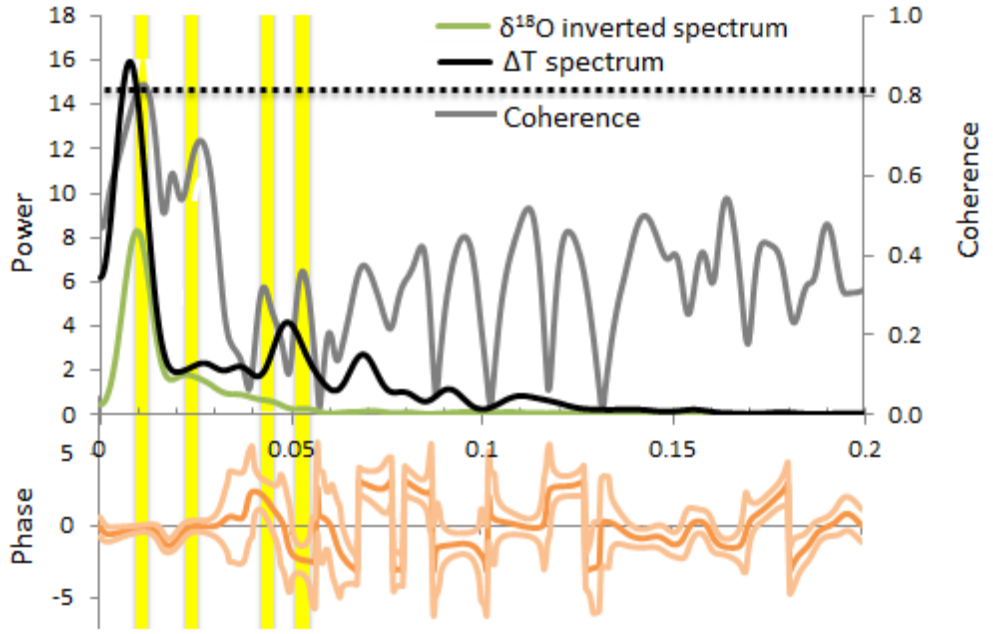

Figure 7 Cross-spectral analysis of $\delta^{18}O$ and ΔT

Cross-spectral analysis of ML1208-17PC $\delta^{18}O$ (green) and ΔT (black). Coherence is plotted in dark gray; dashed line represents limit of nonzero coherence at 80% confidence interval. Phase is plotted in orange with upper and lower bounds plotted in light orange. Yellow bars indicate frequency band for orbital cycles at 100ky, 41ky, 23ky, and 19ky. The two records are coherent and in-phase from 83 to 111ky.

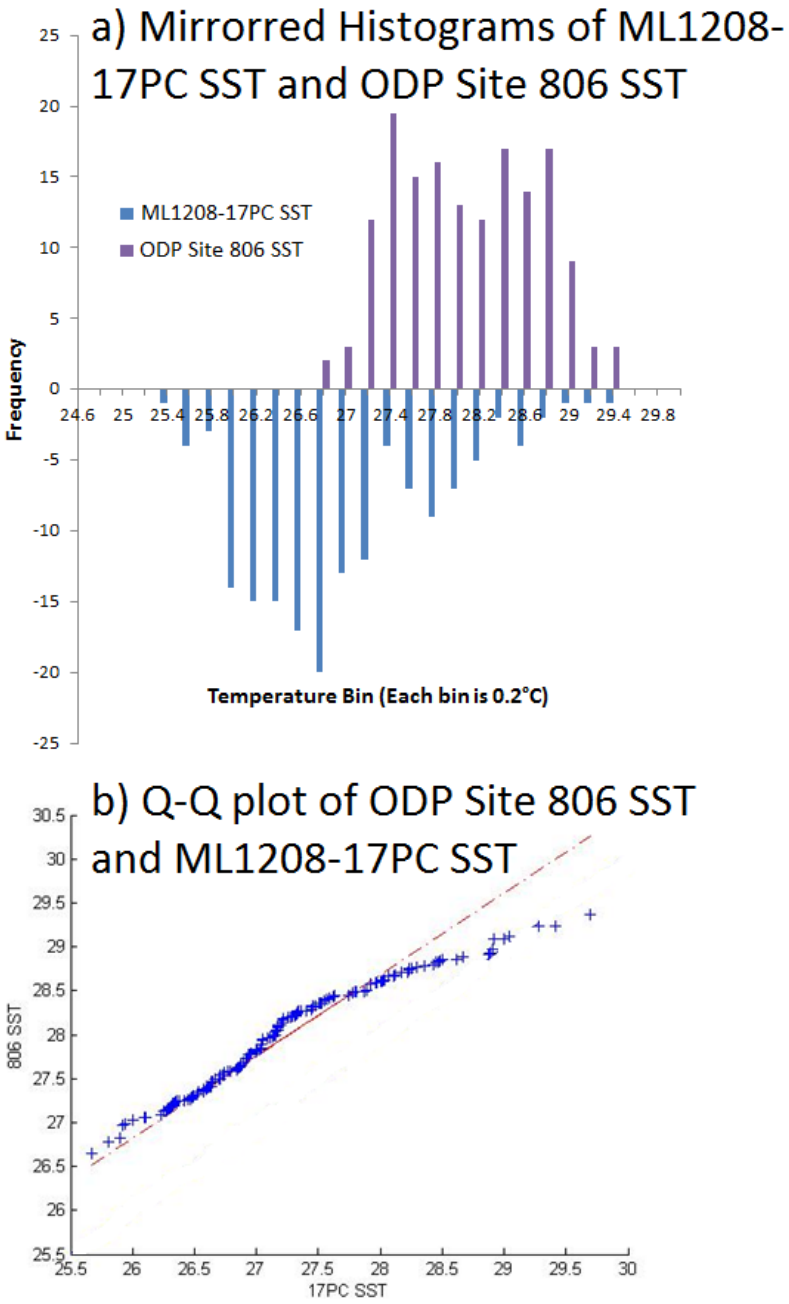

Figure 8 ODP Site 806 SST Histograms and Q-Q plot
a) Mirrored histograms of ODP Site 806 SSTs and ML1208-17PC SSTs with 0.2°C bins. The warmest temperatures converge. b) The Q-Q plot illustrates how ML1208-17PC SSTs warmed more than ODP Site 806 SSTs.

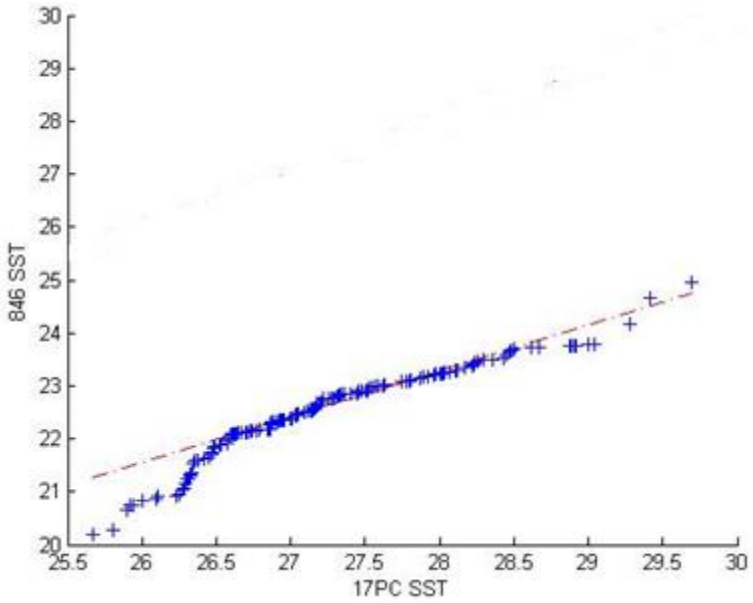

Figure 9 ODP Site 846 and ML1208-17PC SST Q-Q plot
The Q-Q plot of ODP Site 846 and ML1208-17PC SSTs illustrates how ML1208-17PC SSTs cooled less than ODP Site 846 SSTs.

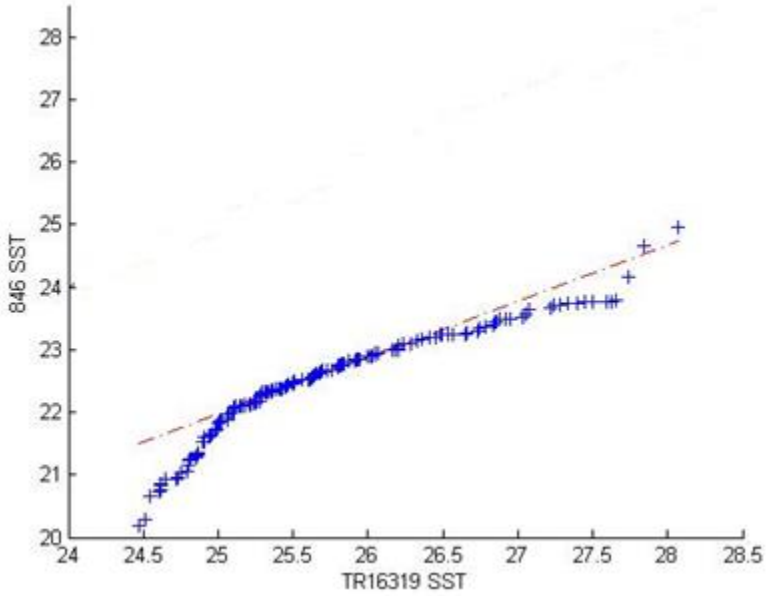

Figure 10 ODP Site 846 and TR163-19 SST Q-Q plot
The Q-Q plot of ODP Site 846 and TR163-19 SSTs illustrates how TR163-19 SSTs cooled less than ODP Site 846 SSTs.

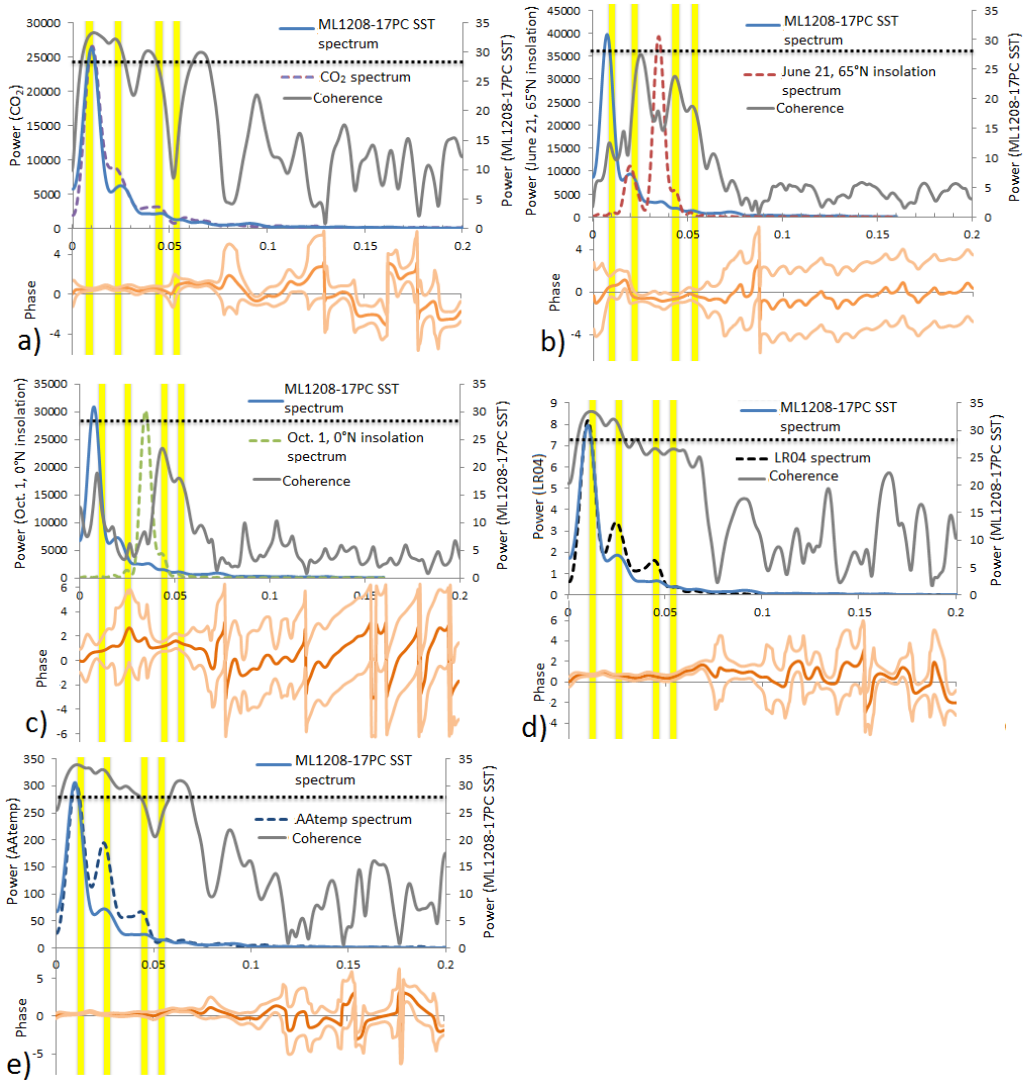

Figure 11a-e Cross-spectral analysis of ML1208-17PC SST (blue) with climate forcings. Coherence is plotted in dark gray; dashed line represents limit of nonzero coherence at 80% confidence interval. Phase is plotted in orange with upper and lower bounds plotted in light orange. When phase is positive, ML1208-17PC SST leads. Yellow bars indicate frequency band for orbital cycles at 100ky, 41ky, 23ky, and 19ky. a) Cross-spectral analysis of ML1208-17PC SST and CO_2 (dashed purple), b) high latitude summer insolation (dashed red), c) local late autumn insolation (dashed green), d) remote ice sheets (LR04, dashed black), e) Antarctic temperature (AAtemp, dashed dark blue).

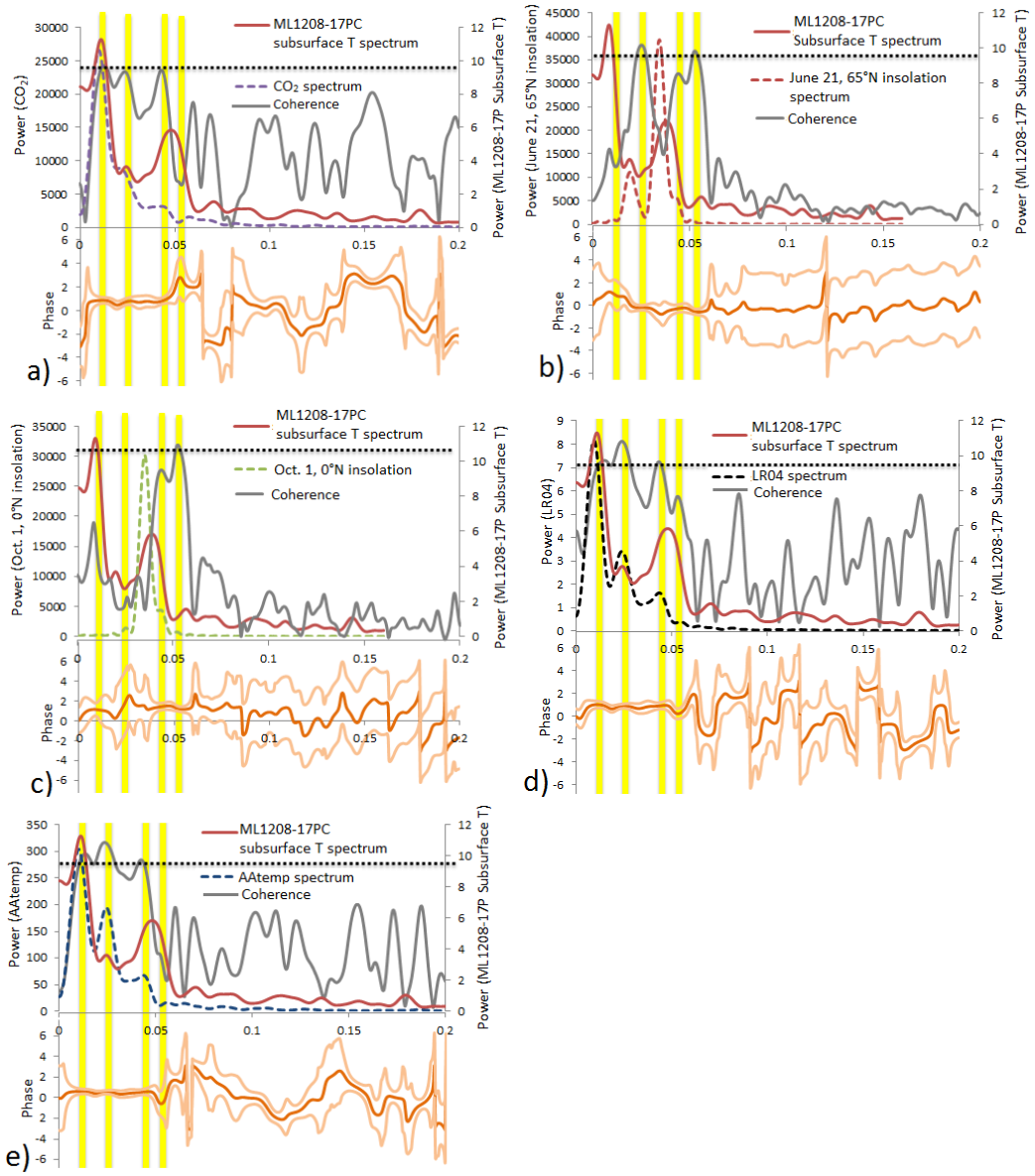

Figure 12a-e Cross-spectral analysis of ML1208-17PC Subsurface temperature (red) with climate forcings. Coherence is plotted in dark gray; dashed line represents limit of nonzero coherence at 80% confidence interval. Phase is plotted in orange with upper and lower bounds plotted in light orange. When phase is positive, ML1208-17PC Subsurface temperature leads. Yellow bars indicate frequency band for orbital cycles at 100ky, 41ky, 23ky, and 19ky. a) Cross-spectral analysis of ML1208-17PC SST and CO_2 (dashed purple), b) high latitude summer insolation (dashed red), c) local late autumn insolation (dashed green), d) remote ice sheets (LR04, dashed black), e) Antarctic temperature (AAtemp, dashed dark blue).

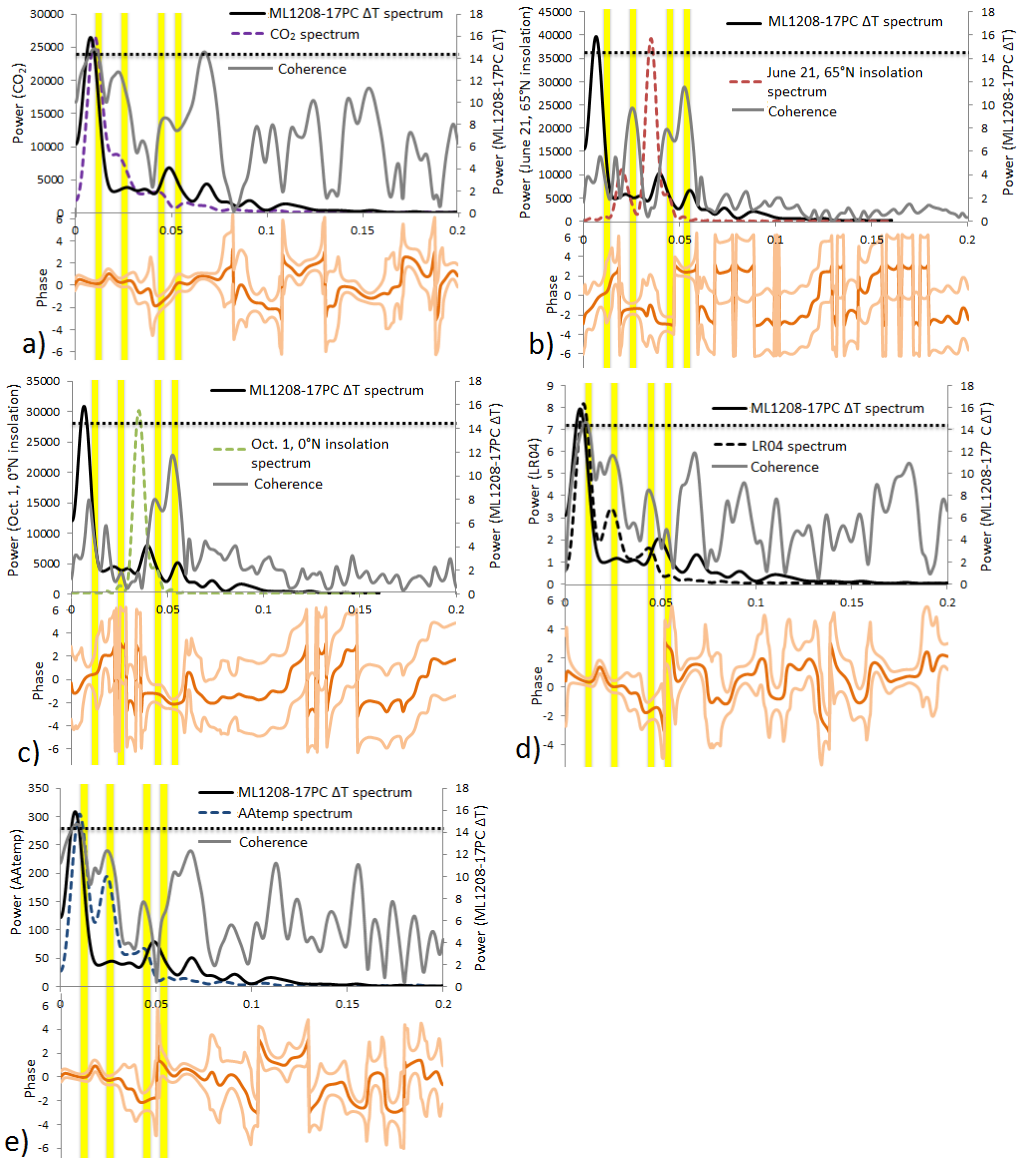

Figure 13a-e Cross-spectral analysis of ML1208-17PC ΔT (black) with climate forcings. Coherence is plotted in dark gray; dashed line represents limit of nonzero coherence at 80% confidence interval. Phase is plotted in orange with upper and lower bounds plotted in light orange. When phase is positive, ML1208-17PC SST leads. Yellow bars indicate frequency band for orbital cycles at 100ky, 41ky, 23ky, and 19ky. a) Cross-spectral analysis of ML1208-17PC SST and CO_2 (dashed purple), b) high latitude summer insolation (dashed red), c) local late autumn insolation (dashed green), d) remote ice sheets (LR04, dashed black), e) Antarctic temperature (AAtemp, dashed dark blue).

APPENDIX A. SUPPLEMENTAL TABLES

Table S-1 ML1208-17PC Age Model

Depth (cm)	Age (ky)
0.00	4.03
33.64	14.84
301.80	117.85
336.93	133.50
469.71	193.90
534.15	232.33
562.78	244.29
648.94	308.20
701.13	338.48
768.23	382.53

Table S-2 ML1208-17PC *G. ruber* Raw Mg/Ca Data and Temperature Calibration

Depth (cm)	Age (ky)	*G. ruber* Mn/Ca (mmol/mol)	*G. ruber* Mg/Ca (mmol/mol)	*G. ruber* T (°C, Dyez and Ravelo 2013 T calibration)
0.00	4.03	0.01	3.27	27.61
4.00	5.32	0.01	3.43	28.00
7.00	6.28	0.01	3.24	27.55
9.00	6.92	0.01	3.19	27.42
12.00	7.89	0.02	3.84	28.92
15.00	8.85	0.03	3.52	28.22
18.00	9.81	0.06	3.12	27.24
22.00	11.10	0.03	3.12	27.24
25.00	12.06	0.02	3.60	28.40
28.00	13.03	0.02	3.36	27.84
32.00	14.31	0.02	3.40	27.95
36.00	15.75	0.02	3.26	27.60
40.00	17.28	0.03	2.97	26.86
44.00	18.82	0.04	2.74	26.24
48.00	20.36	0.04	2.56	25.75
53.00	22.28	0.05	2.62	25.91
56.00	23.43	0.05	2.71	26.18
60.00	24.97	0.05	2.70	26.13
64.00	26.50	0.07	3.00	26.94

67.00	27.66	0.07	3.25	27.57
72.00	29.58	0.06	2.87	26.60
76.00	31.11	0.06	2.61	25.88
80.00	32.65	0.05	2.46	25.46
84.00	34.19	0.07	2.72	26.20
88.00	35.72	0.05	2.66	26.03
92.00	37.26	0.06	2.59	25.83
96.00	38.80	0.07	2.64	25.97
100.00	40.33	0.06	2.74	26.25
104.00	41.87	0.08	2.67	26.04
107.00	43.02	0.05	2.90	26.68
111.00	44.56	0.07	2.67	26.05
116.00	46.48	0.06	2.60	25.86
120.00	48.02	0.07	2.85	26.55
124.00	49.55	0.07	2.64	25.98
132.00	52.63	0.08	2.85	26.54
136.00	54.16	0.07	2.57	25.76
140.00	55.70	0.07	2.51	25.59
144.00	57.24	0.07	2.67	26.05
148.00	58.77	0.07	2.87	26.60
152.00	60.31	0.07	2.66	26.04
156.00	61.85	0.07	2.80	26.42
160.00	63.38	0.07	2.78	26.37
164.00	64.92	0.07	2.70	26.15
168.00	66.46	0.07	2.68	26.08
172.00	67.99	0.07	2.57	25.78
176.00	69.53	0.07	2.86	26.59
188.00	74.14	0.06	2.49	25.53
192.00	75.67	0.07	2.89	26.66
194.00	76.44	0.09	2.66	26.02
196.00	77.21	0.08	2.52	25.63
204.00	80.28	0.06	2.92	26.73
208.00	81.82	0.06	2.71	26.16
212.00	83.36	0.06	3.12	27.25
216.00	84.89	0.06	2.89	26.67
220.00	86.43	0.07	3.11	27.23
224.00	87.97	0.07	3.08	27.16
232.00	91.04	0.05	2.80	26.41
236.00	92.58	0.06	3.19	27.42

244.00	95.65	0.07	3.12	27.24
248.00	97.19	0.06	2.90	26.68
252.00	98.72	0.08	3.15	27.34
256.00	100.26	0.06	3.08	27.15
260.00	101.80	0.07	3.20	27.44
264.00	103.33	0.07	3.06	27.10
268.00	104.87	0.04	2.61	25.89
268.00	104.87	0.04	2.68	26.09
272.00	106.41	0.08	2.90	26.69
276.00	107.94	0.07	3.07	27.12
280.00	109.48	0.08	3.01	26.96
292.00	114.09	0.06	3.21	27.48
304.00	118.82	0.06	3.71	28.64
308.00	120.62	0.06	4.01	29.29
308.00	120.62	0.05	3.83	28.92
312.00	122.41	0.07	3.51	28.19
315.00	123.76	0.06	3.49	28.14
320.00	126.00	0.05	3.77	28.77
324.00	127.80	0.06	3.88	29.02
327.00	129.15	0.03	3.72	28.66
331.00	130.94	0.06	3.91	29.09
335.00	132.68	0.05	3.88	29.02
340.00	134.89	0.05	3.55	28.29
344.00	136.70	0.04	3.45	28.06
348.00	138.52	0.04	3.01	26.96
352.00	140.34	0.05	3.07	27.11
356.00	142.16	0.06	3.06	27.09
364.00	145.80	0.06	2.96	26.84
368.00	147.62	0.06	2.87	26.59
372.00	149.44	0.06	2.86	26.58
376.00	151.26	0.07	3.01	26.98
380.00	153.08	0.07	3.10	27.21
384.00	154.90	0.07	3.04	27.05
388.00	156.72	0.07	3.17	27.38
392.00	158.54	0.07	2.96	26.84
396.00	160.36	0.07	2.72	26.20
396.00	160.36	0.07	2.99	26.93
400.00	162.18	0.07	2.98	26.88
404.00	164.00	0.07	2.95	26.82

408.00	165.82	0.07	2.96	26.84
408.00	165.82	0.07	2.87	26.62
412.00	167.64	0.07	2.84	26.51
415.00	169.01	0.06	2.79	26.40
420.00	171.28	0.06	2.70	26.14
424.00	173.10	0.06	2.88	26.63
428.00	174.92	0.07	2.88	26.63
432.00	176.74	0.06	2.77	26.34
436.00	178.56	0.08	2.76	26.30
440.00	180.38	0.08	2.90	26.68
440.00	180.38	0.07	2.78	26.36
444.00	182.20	0.07	2.74	26.26
448.00	184.02	0.08	2.74	26.24
452.00	185.84	0.06	2.98	26.88
456.00	187.66	0.06	2.90	26.69
460.00	189.48	0.06	2.87	26.61
476.00	197.66	0.07	3.53	28.23
480.00	200.05	0.06	3.51	28.19
480.00	200.05	0.05	3.57	28.33
496.00	209.60	0.06	3.18	27.40
496.00	209.60	0.06	3.45	28.04
500.00	211.99	0.06	3.38	27.89
504.00	214.38	0.06	3.41	27.97
508.00	216.77	0.06	3.59	28.37
512.00	219.16	0.06	3.45	28.05
517.00	222.09	0.06	3.02	26.99
522.00	225.02	0.05	2.85	26.56
530.00	229.69	0.05	3.14	27.30
539.00	234.52	0.05	3.29	27.67
542.00	235.75	0.05	3.44	28.04
546.00	237.40	0.06	3.13	27.28
546.00	237.40	0.06	3.58	28.35
550.00	239.05	0.06	3.46	28.08
555.00	241.11	0.06	3.82	28.88
558.00	242.35	0.05	3.82	28.89
562.00	244.14	0.05	3.23	27.52
567.00	247.43	0.05	3.01	26.96
570.00	249.66	0.05	2.87	26.61
574.00	252.63	0.05	2.85	26.56

578.00	255.60	0.05	2.97	26.88
582.00	258.57	0.05	2.97	26.86
586.00	261.55	0.06	3.25	27.57
590.00	264.52	0.06	3.06	27.09
594.00	267.49	0.06	2.90	26.70
598.00	270.46	0.06	2.88	26.62
602.00	273.43	0.05	2.83	26.50
606.00	276.40	0.05	2.74	26.26
610.00	279.38	0.03	2.97	26.87
622.00	288.29	0.06	3.07	27.13
626.00	291.26	0.05	3.22	27.50
630.00	294.24	0.04	3.29	27.67
634.00	297.21	0.05	2.98	26.89
638.00	300.03	0.06	3.03	27.02
641.00	302.13	0.06	3.11	27.22
645.00	304.93	0.07	3.30	27.70
650.00	308.43	0.05	3.21	27.47
654.00	311.06	0.06	3.20	27.45
657.00	312.81	0.07	3.20	27.44
674.00	322.70	0.06	3.62	28.45
677.00	324.45	0.07	3.68	28.58
680.00	326.19	0.07	3.47	28.10
684.00	328.52	0.08	3.71	28.63
688.00	330.85	0.05	3.89	29.03
692.00	333.17	0.05	4.09	29.46
696.00	335.50	0.05	4.26	29.80
700.00	337.83	0.03	3.90	29.06
704.00	340.37	0.03	3.23	27.53
720.00	350.8742	0.04	2.98	26.90
724.00	353.5003	0.05	2.85	26.54
730.00	357.4394	0.05	2.92	26.73
732.00	358.7524	0.04	2.73	26.21
740.00	364.0045	0.05	2.78	26.36
744.00	366.6305	0.05	2.83	26.50
752.00	371.8826	0.05	2.84	26.52
756.00	374.5087	0.07	2.83	26.49
760.00	377.1347	0.06	2.62	25.91
764.00	379.7608	0.07	2.74	26.26
768.00	382.3868	0.06	3.22	27.51

772.00	385.0129	0.07	2.82	26.47
778.00	388.9519	0.06	3.03	27.03

Table S-3 ML1208-17PC *G.tumida* Raw Mg/Ca Data and Temperature Calibration

Depth (cm)	Age (ky)	*G. tumida* Mn/Ca (mmol/mol)	*G. tumida* Mg/Ca (mmol/mol)	*G. tumida* T (°C, Anand T calibration with Regenberg dissolution correction)
0.00	4.03	0.02	1.75	21.88
4.00	5.32	0.01	1.72	21.77
7.00	6.28	0.01	1.50	20.83
9.00	6.92	0.01	1.38	20.26
12.00	7.89	0.01	1.85	22.30
15.00	8.85	0.01	1.83	22.18
18.00	9.81	0.01	1.24	19.59
22.00	11.10	0.01	1.56	21.10
25.00	12.06	0.01	1.60	21.23
28.00	13.03	0.01	1.67	21.53
32.00	14.31	0.01	1.65	21.45
36.00	15.75	0.01	1.29	19.84
40.00	17.28	0.01	1.65	21.48
44.00	18.82	0.02	1.45	20.59
48.00	20.36	0.02	1.49	20.76
53.00	22.28	0.02	1.46	20.63
56.00	23.43	0.01	1.29	19.82
60.00	24.97	0.02	1.38	20.26
64.00	26.50	0.02	1.49	20.75
72.00	29.58	0.02	1.49	20.77
76.00	31.11	0.01	1.35	20.10
80.00	32.65	0.02	1.33	20.04
84.00	34.19	0.02	1.42	20.42
88.00	35.72	0.02	1.45	20.56
92.00	37.26	0.02	1.62	21.32
96.00	38.80	0.02	1.50	20.80
100.00	40.33	0.02	1.50	20.82
104.00	41.87	0.02	1.40	20.34
107.00	43.02	0.02	1.38	20.25
111.00	44.56	0.01	1.40	20.33
116.00	46.48	0.02	1.67	21.54

120.00	48.02	0.02	1.51	20.88
124.00	49.55	0.02	1.45	20.59
128.00	51.09	0.02	1.53	20.94
132.00	52.63	0.03	1.81	22.13
136.00	54.16	0.04	1.54	20.97
140.00	55.70	0.02	1.38	20.28
144.00	57.24	0.02	1.52	20.92
148.00	58.77	0.02	1.49	20.76
152.00	60.31	0.02	1.52	20.91
156.00	61.85	0.02	1.51	20.88
160.00	63.38	0.02	1.51	20.85
164.00	64.92	0.02	1.64	21.42
168.00	66.46	0.02	1.44	20.53
172.00	67.99	0.01	1.33	20.01
176.00	69.53	0.02	1.43	20.48
180.00	71.06	0.02	1.29	19.81
184.00	72.60	0.01	1.19	19.31
188.00	74.14	0.03	1.48	20.72
192.00	75.67	0.02	1.30	19.88
196.00	77.21	0.01	1.35	20.10
200.00	78.75	0.02	1.64	21.43
204.00	80.28	0.02	1.77	21.96
208.00	81.82	0.02	1.51	20.84
212.00	83.36	0.02	1.59	21.19
216.00	84.89	0.01	1.50	20.80
220.00	86.43	0.01	1.55	21.04
224.00	87.97	0.01	1.41	20.42
228.00	89.50	0.01	1.30	19.89
232.00	91.04	0.01	1.33	20.02
236.00	92.58	0.01	1.19	19.34
240.00	94.11	0.02	1.40	20.36
244.00	95.65	0.01	1.55	21.02
248.00	97.19	0.01	1.37	20.20
252.00	98.72	0.01	1.19	19.33
256.00	100.26	0.01	1.54	21.00
260.00	101.80	0.02	1.50	20.83
264.00	103.33	0.01	1.49	20.75
268.00	104.87	0.01	1.57	21.12
272.00	106.41	0.02	1.50	20.79

276.00	107.94	0.01	1.42	20.45
280.00	109.48	0.02	1.37	20.19
284.00	111.02	0.01	1.44	20.55
292.00	114.09	0.01	1.28	19.76
296.00	115.63	0.01	1.26	19.69
300.00	117.16	0.02	1.51	20.87
304.00	118.82	0.02	1.47	20.67
308.00	120.62	0.01	1.86	22.30
312.00	122.41	0.02	1.63	21.40
315.00	123.76	0.02	1.89	22.45
320.00	126.00	0.02	1.45	20.56
324.00	127.80	0.01	1.22	19.48
327.00	129.15	0.02	1.86	22.33
331.00	130.94	0.02	1.54	20.98
335.00	132.68	0.01	1.68	21.59
340.00	134.89	0.02	1.83	22.20
344.00	136.70	0.02	1.63	21.37
348.00	138.52	0.02	1.55	21.05
352.00	140.34	0.02	1.52	20.88
356.00	142.16	0.02	1.48	20.70
364.00	145.80	0.03	1.49	20.75
368.00	147.62	0.02	1.58	21.18
372.00	149.44	0.02	1.42	20.44
376.00	151.26	0.02	1.43	20.51
380.00	153.08	0.02	1.53	20.94
384.00	154.90	0.02	1.41	20.39
388.00	156.72	0.03	1.61	21.29
392.00	158.54	0.03	1.60	21.26
396.00	160.36	0.03	1.76	21.93
400.00	162.18	0.02	1.58	21.17
404.00	164.00	0.03	1.45	20.60
408.00	165.82	0.02	1.45	20.58
412.00	167.64	0.02	1.47	20.66
415.00	169.01	0.02	1.59	21.19
420.00	171.28	0.02	1.10	18.86
424.00	173.10	0.02	1.31	19.92
428.00	174.92	0.02	1.53	20.95
432.00	176.74	0.03	1.48	20.72
436.00	178.56	0.03	1.65	21.46

440.00	180.38	0.03	1.74	21.85
444.00	182.20	0.02	1.41	20.40
448.00	184.02	0.02	1.56	21.06
452.00	185.84	0.02	1.41	20.40
456.00	187.66	0.01	1.36	20.15
460.00	189.48	0.01	1.21	19.42
464.00	191.30	0.02	1.44	20.54
468.00	193.12	0.02	1.45	20.60
472.00	195.27	0.02	1.46	20.61
476.00	197.66	0.02	1.86	22.33
480.00	200.05	0.01	1.53	20.95
484.00	202.44	0.01	1.56	21.09
488.00	204.82	0.02	1.74	21.84
492.00	207.21	0.01	1.59	21.22
496.00	209.60	0.02	1.63	21.39
500.00	211.99	0.02	1.78	22.01
504.00	214.38	0.03	1.73	21.78
508.00	216.77	0.02	1.70	21.67
512.00	219.16	0.02	2.02	22.95
517.00	222.09	0.02	1.64	21.43
522.00	225.02	0.02	1.62	21.35
526.00	227.36	0.02	1.22	19.49
530.00	229.69	0.01	1.51	20.84
534.00	232.03	0.01	1.60	21.26
539.00	234.52	0.01	1.81	22.12
542.00	235.75	0.01	1.86	22.33
546.00	237.40	0.02	1.88	22.39
550.00	239.05	0.02	1.68	21.58
555.00	241.11	0.02	2.17	23.49
558.00	242.35	0.02	1.83	22.19
562.00	244.14	0.02	1.91	22.51
567.00	247.43	0.02	1.61	21.29
570.00	249.66	0.02	1.52	20.89
574.00	252.63	0.02	1.72	21.75
578.00	255.60	0.02	1.60	21.25
582.00	258.57	0.02	1.65	21.46
586.00	261.55	0.01	1.49	20.78
590.00	264.52	0.03	1.99	22.80
594.00	267.49	0.02	1.62	21.34

598.00	270.46	0.01	1.68	21.61
602.00	273.43	0.01	1.53	20.92
606.00	276.40	0.01	1.44	20.54
610.00	279.38	0.01	1.42	20.43
614.00	282.35	0.01	1.33	20.03
618.00	285.32	0.01	1.49	20.76
622.00	288.29	0.02	1.82	22.15
626.00	291.26	0.01	1.47	20.66
630.00	294.24	0.01	1.60	21.27
634.00	297.21	0.01	1.56	21.10
638.00	300.03	0.01	1.35	20.12
641.00	302.13	0.01	1.55	21.04
645.00	304.93	0.01	1.56	21.08
650.00	308.43	0.02	1.57	21.12
654.00	311.06	0.02	1.70	21.66
657.00	312.81	0.02	1.84	22.26
661.00	315.14	0.01	1.54	21.01
665.00	317.46	0.02	1.41	20.39
670.00	320.37	0.01	1.45	20.57
674.00	322.70	0.02	1.98	22.79
677.00	324.45	0.02	1.73	21.80
680.00	326.19	0.03	1.60	21.25
684.00	328.52	0.03	1.96	22.69
688.00	330.85	0.02	2.07	23.10
692.00	333.17	0.02	1.93	22.59
696.00	335.50	0.02	1.95	22.66
700.00	337.83	0.02	1.91	22.52
704.00	340.37	0.02	1.46	20.63
708.00	343.00	0.02	1.46	20.63
712.00	345.62	0.02	1.30	19.85
716.00	348.25	0.01	1.39	20.32
720.00	350.87	0.02	1.45	20.57
724.00	353.50	0.02	1.47	20.66
728.00	356.13	0.02	1.49	20.76
730.00	357.44	0.02	1.34	20.06
732.00	358.75	0.02	1.32	19.99
740.00	364.00	0.01	1.21	19.41
744.00	366.63	0.02	1.35	20.11
748.00	369.26	0.02	1.37	20.22

752.00	371.88	0.02	1.32	19.95
756.00	374.51	0.02	1.77	21.94
760.00	377.13	0.01	1.38	20.25
764.00	379.76	0.01	1.29	19.82
768.00	382.39	0.02	1.41	20.39
772.00	385.01	0.02	1.51	20.86
778.00	388.95	0.01	1.43	20.49

Table S-4 Summary of Climate Forcings
This table summarizes the phase relationships for SST, subsurface temperature (tumidaT), and ΔT when coherency is greater than 80% with the following climate forcings: CO_2, high latitude summer insolation, local late autumn insolation, remote ice sheets, and Antarctic temperatures. * indicates weaker coherency (>75%).

	CO_2	June 21, 65°N insolation
SST	37 to 200ky: SST leads by 4.8 to 8.8ky	*37 to 41.7ky: SST lags by 5.4 to 1.7ky
	23 to 28ky: SST leads by 1.2 to 3ky	
	14.3 to 16.3ky: SST leads by 1.9 to 3ky	
Subsurface Temperature (tumidaT)	69 to 87ky: tumidaT leads by 7.5 to 13.9ky	36.4 to 44.4ky: tumidaT is in phase -2.9 to 0.2ky
		18.5 to 19.4ky: tumidaT lags by 2.5 to 0.9ky
ΔT	87 to 133.3ky: ΔT is in phase -1.1 to 7.6ky	No coherence
	14.7 to 15.2ky: ΔT leads by 1.4 to 2.6ky	

Oct. 1, 0°N insolation	LR04	AAtemp
No coherence	23.3 to 400ky: SST leads by 1.6 to 5.5ky	23.3 to 400ky: SST leads by 1.6 to 5.5ky
	14.3 to 17.1ky: SST leads by 1.5 to 2.6ky	14.3 to 17.1ky: SST leads by 1.5 to 2.6ky
18.7 to 19.4ky: tumidaT leads by 2.9 to 4.4ky	36.5 to 50ky: tumidaT leads by 4.1 to 7.1ky	60.9 to 90.9ky: tumidaT leads by 4.1 to 9.9ky
		35.1 to 52.6ky: tumidaT leads by 1.9 to 4.8ky
		23 to 24.1ky: tumidaT leads by 1 to 3ky
No coherence	83.3 to 111.1ky: ΔT leads by 2.2 to 10ky	95.2 to 153.8ky: ΔT is in phase -3.9 to 6ky

REFERENCES

Anand, P., H. Elderfield, and M. H. Conte, Calibration of Mg/Ca thermometry in planktonic foraminifera from a sediment trap time series, Paleoceanography, 18(2), 1050, doi:10.1029/2002PA000846, 2003.

Adler, R. F. et al. (2003), The Version-2 Global Precipitation Climatology Project (GPCP) monthly precipitation analysis (1979–present), *J. Hydrometeorol.*, 4, 1147–1167, doi.org/10.1175/1525-7541(2003)004<1147:TVGPCP>2.0.CO;2.

Anand, P., H. Elderfield, and M. H. Conte, Calibration of Mg/Ca thermometry in planktonic foraminifera from a sedimenttrap time series, *Paleoceanography*, 18(2), 1050, doi:10.1029/2002PA000846, 2003.

Andreasen, D. H., and A. C. Ravelo (1997), Tropical Pacific Ocean thermocline depth reconstructions for the last glacial maximum, *Paleoceanography*, 12(3), 395–413, doi:10.1029/97PA00822.

Boyle, E. A., and L. D. Keigwin (1985), Comparison of Atlantic and Pacific paleochemical records for the last 215,000 years: Changes in deep ocean circulation and chemical inventories, *Earth Planet. Sci. Lett.*, 76(1–2), 135–150, doi:10.1016/0012-821X(85)90154-2.

Cane, M. A. (1998), A role for the tropical Pacific, *Science*, 282(5386), 59–61, doi:10.1126/science.282.5386.59.

Dyez, K., and A. C. Ravelo (2013), Late Pleistocene tropical Pacific temperature sensitivity to radiative greenhouse gas forcing, *Geology*, 41(1), 23–26, doi:10.1130/G33425.1.

Dyez, K., and A. C. Ravelo (2014), Dynamical changes in the tropical Pacific warm pool and zonal SST gradient during the Pleistocene, *Geophys. Res. Lett.*, 41, 7626–7633, doi:10.1002/2014GL061639.

Dyez, K. A., A. C. Ravelo, and A. C. Mix (2016), Evaluating drivers of Pleistocene eastern tropical Pacific sea surface temperature, *Paleoceanography*, 31, 1054–1069, doi:10.1002/2015PA002873.

Herbert, T. D., L. C. Peterson, K. T. Lawrence, and Z. Liu (2010), Tropical ocean temperatures over the past 3.5 million years, *Science*, 328, 1530–1534, doi:10.1126/science.1185435.

Jouzel, J., et al. (2007), Orbital and millennial Antarctic climate variability over the past 800,000 years, *Science*, 317(5839), 793–796, doi:10.1126/science.1141038.

Lea, D. W. (2004), The 100 000-yr cycle in tropical SST, greenhouse forcing, and climate sensitivity, *J. Clim.*, 17(11), 2170–2179, doi:10.1175/1520-0442(2004)017<2170:TYCITS>.

Lea, D. W., D. K. Pak, C. L. Belanger, H. J. Spero, M. A. Hall, and N. J. Shackleton (2006), Paleoclimate history of Galapagos surface waters over the last 135,000 yr, *Quat. Sci. Rev.*, 25(11-12), 1152–1167, doi:10.1016/j.quascirev.2005.11.010.

Lisiecki, L. E., and M. E. Raymo (2005), A Pliocene-Pleistocene stack of 57 globally distributed benthic δ18O records, *Paleoceanography*, 20, PA1003, doi:10.1029/2004PA001071.

Liu, Z., and T. D. Herbert (2004), High-latitude influence on the eastern equatorial Pacific climate in the early Pleistocene epoch, *Nature*, 427(6976), 720–723, doi:10.1038/nature02338.

Lynch-Stieglitz, J., et al. (2015), Glacial-interglacial changes in central tropical Pacific surface seawater property gradients, *Paleoceanography*, 30, doi:10.1002/2014PA002746.

Martinez-Garcia, A et al. (2010): Subpolar Link to the Emergence of the Modern Equatorial Pacific Cold Tongue. *Science*, 328(5985), 1550-1553, doi.org/10.1126/Science.1184480

Mashiotta, T., D. W. Lea, and H. J. Spero (1999), Glacial-interglacial changes in subantarctic sea surface temperature and δ18O-water using foraminiferal Mg, *Earth Planet. Sci. Lett*., 170(4), 417–432, doi:10.1016/S0012-821X(99)00116-8.

Medina-Elizalde, M., and D. W. Lea (2005), The mid-Pleistocene transition in the Tropical Pacific, *Science*, 310(5750), 1009–1012, doi:10.1126/science.1115933.

Mitchell, T. P., and J. M. Wallace (1992), The annual cycle in equatorial convection and sea surface temperature, *J. Clim*., 5, 1140-1156, doi:?

Palliard, D., L. Labeyrie, and P. Yiou (1996), Macintosh program performs time-series analysis, *Eos Trans. AGU*, 77–379.

Patrick, A., and R. C. Thunell (1997), Tropical Pacific sea surface temperatures and upper water column thermal structure during the last glacial maximum, *Paleoceanography*, 12(5), 649-657, doi.org/10.1029/97PA01553.

Philander, S. G., and A. V. Fedorov (2003), Role of tropics in changing the response to Milankovich forcing some three million years ago, *Paleoceanography*, 18(2), 1045, doi:10.1029/2002PA000837.

Ravelo, A. C., and N. J. Shackleton (1995), Evidence for surface-water circulation changes at Site 851 in the eastern tropical pacific ocean, *Proceedings of the Ocean Drilling Program, Scientific Results*, 138, 503-516.

Regenberg, M., A. Regenberg, D. Garbe-Schönberg, and D. W. Lea (2014), Global dissolution effects on planktonic foraminiferal Mg/Ca ratios controlled by the calcite-saturation state of bottom waters, *Paleoceanography*, 29, 127–142, doi:10.1002/2013PA002492.

Schmidtko, S., G. C. Johnson, and J. M. Lyman (2013), MIMOC: A global monthly isopycnal upper-ocean climatology with mixed layers, *J. Geophys. Res. Oceans*, 118, 1658–1672, doi:10.1002/jgrc.20122.

Spero, HJ et al. (2003): Multispecies approach to reconstructing eastern equatorial Pacific thermocline hydrography during the past 360 kyr. *Paleoceanography*, 18(1), 1022, doi.org/10.1029/2002PA000814

Talley, L. D., et al. (2011), Descriptive Physical Oceanography.